J Mater Sci (2007) 42:5581–5588
DOI 10.1007/s10853-006-1095-3

Mechanical properties of electrodeposited nanocrystalline copper using tensile and shear punch tests

Ramesh Kumar Guduru · Kristopher A. Darling · Ronald O. Scattergood · Carl C. Koch · K. L. Murty

Received: 14 April 2006 / Accepted: 2 October 2006 / Published online: 4 April 2007

Abstract Characterization of the mechanical properties of electrodeposited nanocrystalline Cu with an average grain size of 74 nm was carried out using two different testing techniques, shear punch tests and tensile tests. The grain size distribution was broad and the volume fraction of larger grains was appreciable. The electrodeposited Cu had a high yield strength combined with moderate ductility and strain hardening. Scatter in the ductility values was attributed to residual porosity and inhomogeneity in the microstructure. Measurements of the strain rate sensitivity showed a significant increase in the rate sensitivity and a decrease in the activation volume for the deformation of nanocrystalline Cu compared with similar tests on coarse-grained cold worked Cu.

Introduction

The mechanical behavior of nanocrystalline (nc) metals has been a research topic of considerable interest for the past two decades. Researchers [1–6] have investigated the deformation mechanisms of these materials through experimental studies and modeling simulations. The nc metals have attracted attention because of their superior strength properties [7–12] in comparison with their coarse-grained counterparts. Except for a few reports [2, 11, 13, 14], limited ductility is observed in nc Cu [15]. The poor ductility is believed to be largely due to pre-existing flaws, such as porosity, weak inter-particle bonding and chemical impurities [10, 15, 16]. Recently Cheng et al. [2] and Youssef et al. [11] reported high strength as well as superior ductility for ball milled nc copper. These investigators used a combination of room temperature milling and cryomilling to produce in situ consolidation. In [2] the material was shown to have some porosity whereas no artifacts were observed in [11]. The studies done by Lu [17–19] showed increased strength, ductility and strain rate sensitivity in copper with nano-sized twins. The grain size of the twinned copper was in the range of several hundred nanometers; the high strength and rate sensitivity was attributed to the twinned nanostructure and high twin density. The nc Cu produced by Wang et al. [20] by surface mechanical attrition treatment was shown to have high strength but low ductility. Youngdahl [12] and Huang [21] showed that nc Cu produced by the compaction of powders using inert gas condensation had high strength, non-uniform deformation and poor ductility. Lu et al. [13, 14] reported a large amount of ductility and superplastic behavior in electrodeposited nc Cu, but the strength of this material was low. The literature [9, 22–24] shows that nc Cu obtained by an electrodeposition route can have high strength, but usually limited ductility.

Because of sample size restrictions, specialized mechanical property testing techniques are often needed for nc metals [1, 2, 8, 11, 21, 25–28]. In the work reported here, the shear punch test (SPT) and the tensile test are used to characterize the strength and strain rate sensitivity of an nc Cu produced by electrodeposition. The SPT method has been used for testing large grain size metals and alloys [29–37]. It is a very convenient method for preparing and testing small samples. The present work extends the SPT method to an nc metal, and also applies it

R. K. Guduru · K. A. Darling · R. O. Scattergood (✉) · C. C. Koch · K. L. Murty
Department of Materials Science and Engineering, NC State University, Raleigh, NC 27606-7907, USA
e-mail: ron_scattergood@ncsu.edu

to the characterization of strain rate effects. Tensile test results obtained for the same nc Cu provide a useful comparison for validating the SPT results.

Experimental procedure

Material characterization

Electrodeposited nc Cu (enc Cu) was obtained from the 3M corporation in the form of a 200 μm thick sheet. The enc Cu is produced using a proprietary electrodeposition process. The grain size was characterized using transmission electron microscopy (TEM). Fracture surfaces were characterized using scanning electron microscopy (SEM). Chemical analysis of the enc Cu was done by the Northern Analytical Laboratory, Merrimack, NH, USA. The density was determined to be 8.90 ± 0.03 g/cm^3 using Archimedes method (≈99.34% of the theoretical density—8.96 g/cm^3). Coarse grain size (cgs), 99.9% purity Cu was obtained from McMaster Carr, USA in cold rolled sheet form with a thickness of 820 μm. Vickers hardness measurements were made using an average of eight indentations with 50 g load and a dwell time of 15 s. The Vickers hardness values for the enc Cu and the cgs Cu were 2,040 ± 50 MPa and 740 ± 15 MPa, respectively.

Mechanical testing

The shear punch test fixture is shown in Fig. 1a. The effective shear stress τ is defined as

$$\tau = \frac{P}{\pi\, t\, d_{\text{mean}}} \tag{1}$$

P is the punch load, δ is the punch displacement, t is the sample thickness and $d_{\text{mean}} = (d_{\text{die}} + d_{\text{punch}})/2$, where d_{die} is the diameter of the die—2.51 mm and d_{punch} is the diameter of the punch—2.49 mm. The gap between the die and punch is called die–punch clearance zone which is indicated in Fig. 1b as 'c' and this can be defined as $c = (d_{\text{die}} - d_{\text{punch}})/2$. A suitable definition for the effective shear strain has not been established. The strain in the shear zone deviates from pure shear shown in Fig. 1b because of bending effects [30]. For strain rate sensitivity analysis, the effective SPT strain rate is assumed to be proportional to the punch displacement rate $\dot{\delta}$.

A correlation of the form $\sigma = \alpha\tau$ between tensile stress σ and shear stress τ has been proposed for shear punch testing by several investigators [29–35, 37]. Values of α can be obtained for the yield stress and ultimate stress. Details on the correlation methodology for the SPT setup used in the present work are reported elsewhere [29]. The correlations were developed using experimental results and FEA

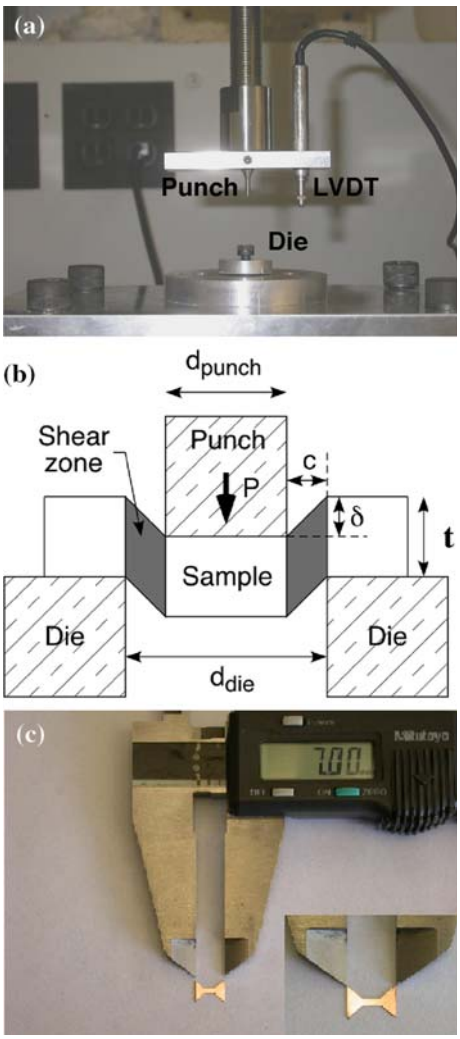

Fig. 1 (**a**) Test setup, (**b**) idealized shear zone geometry and (**c**) mini-tensile sample

simulations [30]. A critical requirement is that at an offset yield point, a through-section plastic zone must be formed in the punch-die clearance region. A 1% offset criterion was established using τ versus normalized punch displacement δ/t curves. The correlations obtained for a representative range of large grain size metals and alloys were

$$\sigma_{0.02} = \alpha\tau_{1.00}, \quad \text{where } \alpha = 1.77 \tag{2a}$$

$$\sigma_{\text{u}} = \beta\tau_{\text{u}}, \quad \text{where } \beta = 1.80 \tag{2b}$$

$\sigma_{0.02}$ and $\tau_{1.00}$ denote the 0.02% tensile offset yield point and the 1.00% SPT normalized displacement offset yield point, measured for a tensile strain rate of 4×10^{-4} s^{-1} and an SPT punch displacement rate of 4.23×10^{-3} mm s^{-1}, respectively. σ_{u} and τ_{u} are the corresponding ultimate stress values at the maximum loads, α and β are the

correlation constants. Standardization of the rates is necessary to account for strain rate sensitivity effects when making specific comparisons.

SPT samples were 5 mm diameter disks cut from enc Cu and cgs Cu sheets. Polishing to obtain parallel surfaces with a mirror finish was carried out on successively finer grades of emery paper with final polishing being done using 0.1 μm alumina slurry on polishing cloth. Five tests were done for testing with a punch displacement rate of 4.23×10^{-3} mm s^{-1}. For strain rate sensitivity evaluation, three tests were done at each of four other rates ranging from 8.47×10^{-4} to 8.47×10^{-2} mm s^{-1}.

Tensile test samples were prepared from enc Cu sheet blanks using a Microproto Systems 2000 CNC micromilling machine with a 1 mm diameter WC milling tool. Tensile tests were not done on the cgs Cu. The length of a dog-bone tensile specimen shown in Fig. 1c is 7 mm, the gauge length is 2 mm and the width is 1 mm. Specimens were polished with successively finer grades of emery paper and alumina slurry to get a mirror finish. Tensile tests were done on a specially designed mini-tensile test machine. Tests were carried out at four strain rates ranging from 2.5×10^{-4} s^{-1} to 2.5×10^{-2} s^{-1}. Strain was determined using the gauge length and strain rates were corrected for machine compliance when needed. Two tests were done at each of the highest and the lowest strain rates and three tests were done at each of the intermediate rates.

The strain rate sensitivity was characterized using tensile tests and shear punch tests done over a range of strain rates and punch displacement rates. Stress relaxation tests were done using the SPT method and a punch displacement rate of 4.23×10^{-4} mm s^{-1}.

Results and discussion

Material characterization

A bright field TEM image and diffraction pattern of the enc Cu is shown in Fig. 2a. The microstructure consists of equiaxed grains with twinning in some grains, as indicated in the figure. The number-average grain size was 74 nm for the distribution shown in Fig. 2b. Due to the spread of the distribution to grain sizes >100 nm, the volume average grain size is increased to 138 nm. Spectroscopic chemical analysis showed that the enc Cu was 99.88% pure and contained 0.0458% C, 0.0197% S, 0.0256% O and 0.0112% N impurities.

Strength properties

Tensile tests and shear punch tests for enc Cu done at different loading rates are shown in Figs. 3 and 4,

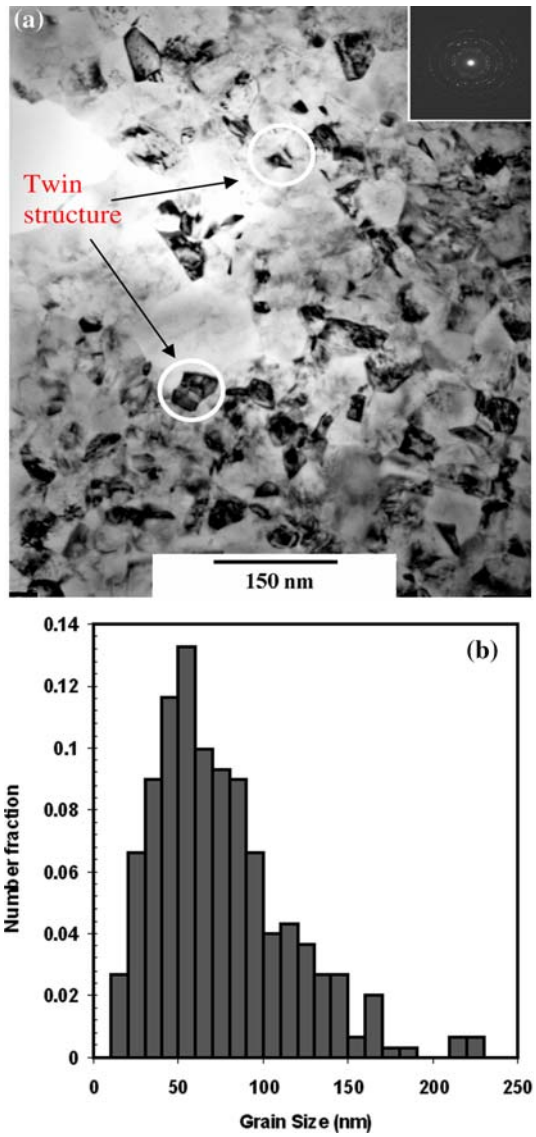

Fig. 2 (**a**) TEM for enc Cu, (**b**) number average grain size distribution

respectively. Figure 4 also shows an SPT curve obtained for cgs Cu in the inset. Table 1 compares the yield stress and ultimate stress values for the shear punch and the tensile tests done at the standard strain rate and punch displacement rate. The correlation results based on the SPT data for enc Cu are shown in the last row in Table 1. The correlation predicts the tensile yield and ultimate stress values for enc Cu to within 6% of the measured values. Taking into account that the experimental scatter in the testing results is about ±2%, this is considered good agreement. The strain-hardening ratio of ultimate/yield stress for enc Cu obtained from the shear punch tests and tensile tests is 1.28 and 1.34, respectively. This can be compared to the ratio 1.63 obtained for cgs Cu from the shear punch test. The tensile ductility of the enc Cu showed

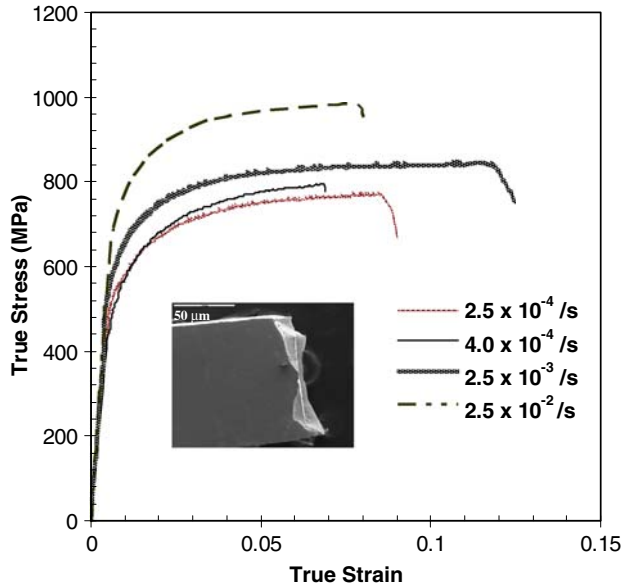

Fig. 3 Tensile tests for enc Cu (sample fracture—inset)

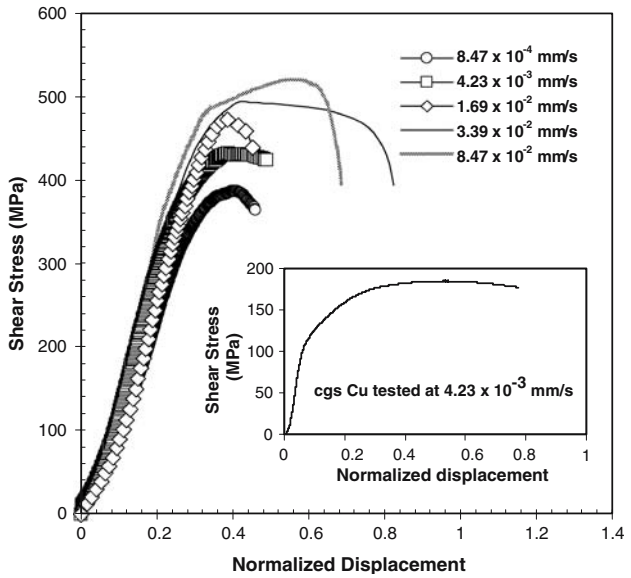

Fig. 4 Shear punch tests for enc Cu and cgs Cu

considerable scatter (Fig. 3), with the variation being about 4–11%.

The tensile strength (~560 MPa yield, ~750 MPa ultimate), hardening ratio (≈1.3) and tensile ductility (≈7.5 ± 3.5%) for the enc Cu exceeds that of other electrodeposited Cu materials reported in the literature [9, 13, 24, 28]. The twinned nanostructure of the electrodeposited Cu (grain size >100 nm) produced by Lu et al. [19] is an exception. Ebrahimi et al. [24] obtained a maximum plastic strain of 2% in electrodeposited nc Cu and enhanced ductility of 6% in annealed samples, but with lower strength. The ductility and strain hardening capacity obtained for our enc Cu could be enhanced by a high volume fraction of large grains (Fig. 3b). Ductility and strain hardening capacity in nc Cu have been attributed to the presence of larger grains within a nanocrystalline matrix [38].

Strain rate sensitivity

In coarse-grained fcc metals, the primary obstacle to the thermally activated motion of mobile dislocations arises from forest dislocation intersections. The parameters that are used for characterizing the deformation kinetics are the strain rate sensitivity m and the activation volume v^*. The strain rate sensitivity m is defined using the phenomenological relation

$$m = \frac{\partial \ln S}{\partial \ln \dot{r}} \tag{3}$$

S and $\dot{r}$ represent the stress and strain rate conjugate variables. These are σ and $\dot{\varepsilon}$ for a tensile test and τ and $\dot{\delta}$ for a shear punch test. The latter assumes that an effective shear strain rate for the SPT is proportional to the punch displacement rate $\dot{\delta}$. Scaling factors for stress or strain rate can be subsumed into fitting constants when logarithmic stresses or strain rates are used.

Thermal activation analysis provides a mechanism-based framework for investigating the strain rate response. For purposes of comparing the results for the shear punch and tensile tests, we adopt a thermal activation model corresponding to a linear relation between the τ_r and the logarithmic strain rate [39]

$$\tau_r = Q + \frac{kT}{v*} \ln \dot{r} \tag{4}$$

τ_r is the resolved shear stress for dislocation slip, T is the absolute temperature, k is Boltzmann's constant, v^* is the apparent activation volume, $\dot{r} = \dot{\varepsilon}$ (tensile strain rate) or $\dot{\delta}$ (punch displacement rate) and Q is a constant. $v^* = bLy_o$, b is Burger's vector, y_oL is the activation area (assumed to be independent of τ_r), L is the activation length and y_o is the obstacle width $\approx b$. Stress relaxation tests can also be used to obtain an apparent activation volume. If the stress change $\Delta\tau_r$ during stress relaxation follows a logarithmic decay with respect to time t, the apparent activation volume is obtained [40] using the relation

$$\Delta\tau_r = -A \ln\left(1 + \frac{t}{C}\right) \tag{5}$$

where $A = kT/v^*$ and C is a time constant.

Table 1 SPT and tensile test results for enc Cu and cg Cu

Material	Shear punch tests		Tensile tests	
	Yield stress (MPa)	Ultimate stress (MPa)	Yield stress (MPa)	Ultimate stress (MPa)
Enc	332 ± 6	424 ± 6	558 ± 9	747 ± 7
Cgs	114 ± 3	186 ± 2	–	–
enc Eq. 2			588 ± 11	763 ± 11

Figure 5 shows the results for the strain rate sensitivity m obtained using a power law relation for Eq. 3 and tensile or SPT yield stresses at the different strain or punch displacement rates. m is larger for enc Cu compared to cgs Cu, consistent with the trends reported by Wei et al. [41]. The values of m for the shear punch and tensile tests using enc Cu differ by about 8%. The difference is comparable to the uncertainty in the fit for the slopes.

Figures 6 and 7 show normalized v^* values (units of b^3) obtained for enc Cu using Eq. 4 and data from tensile and shear punch tests, respectively. The stress at yield, an intermediate strain/displacement point and the ultimate stress were used for determining the v^* values. The resolved shear stress τ_r in Eqs. 4 and 5 was evaluated from the tensile stress σ and the shear punch stress τ using $\sigma = 3\tau_r$ (Taylor factor) and $\tau = \sigma/\alpha = 3\tau_r/\alpha$, respectively, with $\alpha = 1.77$ (see Eq. 2a) For Cu at the ambient test temperature (300 K), $kT/b^3 = 247$ MPa. The SPT v^* values for cgs Cu were $225b^3$ (yield stress), $170b^3$ ($\delta/t = 0.05$) and $120b^3$ (ultimate stress). The v^* values for SPT versus tensile tests in Figs. 6 and 7 differ by 10% or less. The difference is again comparable to the uncertainty in the

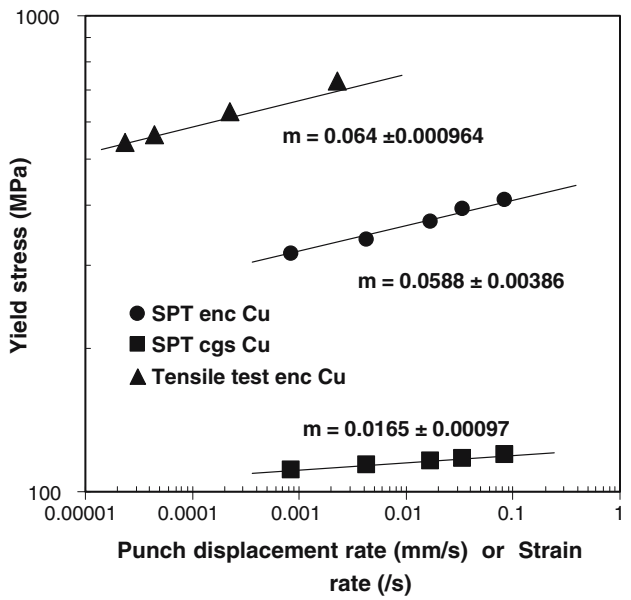

Fig. 5 Log stress versus log strain rate or log punch displacement rate for tensile and SPT yield stress values (m values indicated)

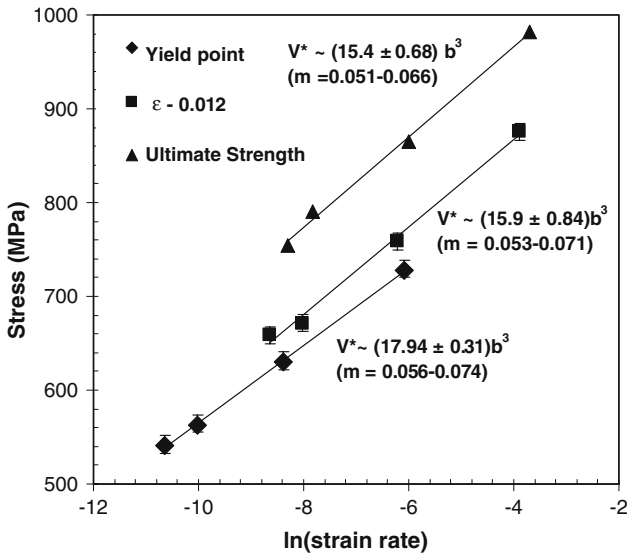

Fig. 6 Stress versus log strain rate and v^* values indicated for tensile tests (m range shown) for enc Cu. The stress value corresponding to $\varepsilon - 0.12$ was taken using an offset from the tensile test data obtained at different strain rates

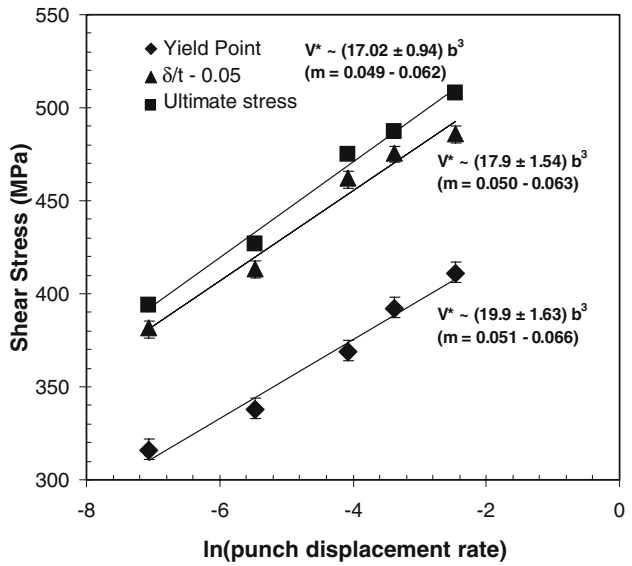

Fig. 7 Stress versus log punch displacement rate and v^* values indicated for SPT (m range shown) for enc Cu. The stress value at $\delta/t - 0.05$ was taken using an offset from the SPT curves obtained at different punch displacement rate tests

slopes. There is much less effect of stress on the SPT v^* values for enc Cu (15%) compared to cgs Cu (50%). This would be consistent with an activation length L determined by grain size for nc metals, as suggested by Wei et al. [41].

The v^* values for the SPT stress relaxation curves shown in Fig. 8 (using Eq. 5 and appropriate conversion factors) are $33b^3$ and $310b^3$ for enc Cu and cgs Cu, respectively. These v^* values are larger by about 50% compared to the SPT values for enc Cu in Fig. 7. Likewise, the v^* for cgs Cu is larger for stress relaxation ($310b^3$ vs. $225b^3$). Differences in the apparent activation volumes obtained from the transient stress relaxation tests and the monotonic strain rate tests can be attributed to changes in microstructural state parameters which are not held fixed from specimen to specimen in monotonic strain rate tests, for example, mobile dislocation density. Cheng et al. [2] determined a true v^* value of $25b^3$ using strain-rate jump tests for an nc Cu with a grain size of 54 nm.

Equations 3 and 4 show that m and v^* are related as

$$m = \frac{\partial \ln S}{\partial \ln \dot{r}} = \frac{kT}{Sv*} \tag{6}$$

If v^* is constant then m cannot be constant (and vice versa), and the linear fits in Fig. 5 and Figs. 6 or 7 cannot be mutually consistent. Assuming a constant v^* as the basis for comparison, the range of m values corresponding to the stress range for each of the plots in Figs. 6 and 7 is indicated. Comparing results obtained using yield stresses, it can be seen that the m values in Fig. 5 are average values for the range of m values required in Figs. 6 and 7.

Wei et al. [41] used the activation length L to rationalize the increase in m as grain size is reduced to the nanoscale for pure fcc metals. For large grain-size metals the Hall Petch effect (strengthening due to grain size change) is minimal and strengthening is assumed to be controlled by the dislocation density ρ. L is identified as the dislocation network spacing where $\rho = 1/L^2$. $\tau_r \propto \sqrt{\rho} = 1/L$ for dislocation strengthening and $m \propto 1/\tau_r L$ would be nominally independent of grain size in this limit. As the grain size reduces to the nanoscale regime, the grain-size strengthening effect dominates. L is now assumed to be proportional to grain size D and $\tau_r \propto 1/D^{1/2}$ for the Hall Petch effect. This gives $m \propto 1/D^{1/2}$ which implies that the strain rate sensitivity of pure fcc metals would increase as the grain size decreases in the nanoscale range. The SPT results for enc Cu and cgs Cu are consistent with this trend.

Fracture surfaces

Figure 9 shows SEM micrographs of the facture surfaces of the tensile (a, b) and SPT (c, d) tested samples. The shear localization failure mode reported by Cheng [2] was not observed in the present nc Cu (Fig. 3 inset). Figure 9a shows a featureless region with fine-scale surface roughness, while Fig. 9b shows a rough morphology resembling a dimpled structure. The same features were found on tensile fracture surfaces of other electrodeposited materials [22–24]. The rough morphology originates from intergranular fracture, and has been associated with higher ductility [22]. This is consistent with a higher fraction of rough morphology (>50%) found in tensile tested samples that showed higher ductility (Fig. 3). Figure 9c, d shows SPT shear fracture surfaces for cgs Cu and enc Cu, respectively. Shear lines in the direction of the punch displacement are evident in both figures. Residual porosity can be observed on the enc Cu shear surface (Fig. 9d). Porosity could not be detected on tensile fracture surfaces of enc Cu, and was obscured possibly by other features. Residual porosity can limit tensile ductility and will contribute to the scatter seen in Fig. 3.

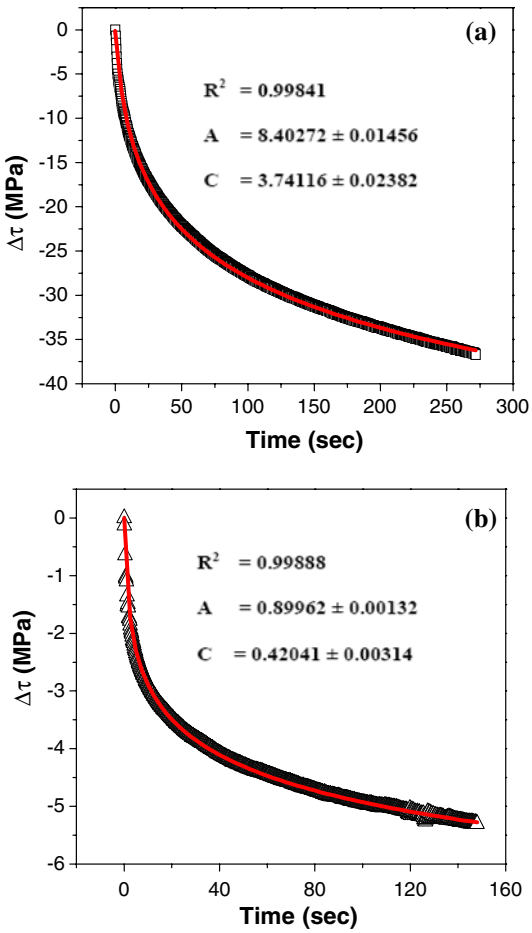

Fig. 8 Stress relaxation test data obtained using SPT: (**a**) on enc Cu, and (**b**) on cgs Cu. The solid line curve fits were obtained using Eq. 5 and also appropriate conversion factors between τ_r (resolved shear stress) and τ (stress in SPT), with C as the fitting parameter

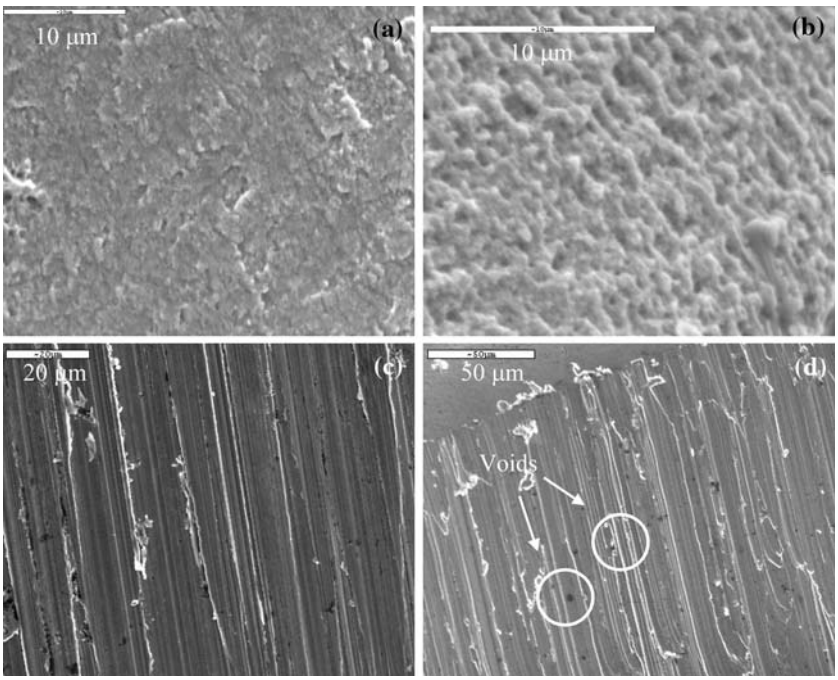

Fig. 9 SEM fracture surfaces (**a**) tensile fracture surface—smooth region, (**b**) tensile surface—rough (dimpled) region, (**c**) SPT shear surface cgs Cu, and (**d**) SPT shear surface enc Cu—voids are indicated (arrows)

Summary and conclusions

The mechanical properties of an enc Cu were characterized using tensile tests and a shear punch test (SPT) technique. The correlation relations for tensile yield and ultimate stresses developed previously for the SPT stresses gave good agreement with the tensile test results on enc Cu. Strain rate sensitivity m and an apparent activation volume v^* were determined using tensile tests and, as far as the authors are aware, measured for the first time using the SPT technique. SPT stress relaxation tests were also done. The range of m values and apparent activation volumes v^* obtained using the SPT method were in general agreement with tensile test results. Differences of the order of 10% were observed. Apparent v^* values for SPT stress relaxation tests were about 50% higher than the other SPT v^* values. The trends in the m and v^* values were consistent with a model proposed in the literature for strain rate effects in pure fcc metals with grain sizes decreasing to the nanoscale. Finally, we conclude from the work reported here that the shear punch test can be a valuable characterization tool for the mechanical properties and strain rate effects of nc metals. Its advantage lies in the ease of sample preparation and the small sample sizes that can be tested.

Acknowledgements The authors are grateful to Dr. Gerd Duscher and Liu Fude for helping with TEM sample preparation. Stefan Sandukas assisted in preparing the mini-tensile samples. We are grateful to Dr. William Bryan (3M corporation) for supplying the electrodeposited nc Cu material. This research was supported by the National Science Foundation, Grant number DMR-0201474.

References

1. Schwaiger R, Moser B, Dao M, Chollacoop N, Suresh S (2003) Acta Mater 51:5159
2. Cheng S, Ma E, Wang YM, Kecskes LJ, Youssef KM, Koch CC, Trociewitz UP, Han K (2005) Acta Mater 53:1521
3. Kumar KS, Van Swygenhoven H, Suresh S (2003) Acta Mater 51:5743
4. Jia D, Ramesh KT, Ma E (2003) Acta Mater 51:3495
5. Schiotz J, DiTolla FD, Jacobsen KW (1998) Nature 391:561
6. Jiang B, Weng GJ (2004) J Mech Phys Solids 52:1125
7. He L, Ma E (1996) Nanostruct Mater 7:327
8. Legros M, Elliott BR, Rittner MN, Weertman JR, Hemker KJ (2000) Phil Mag A 80(4):1017
9. Ebrahimi F, Zhai Q (1998) Scr Mater 39:1401
10. Sanders PG, Youngdahl CJ, Weertman JR (1997) Mater Sci Eng A 234–236:77
11. Youssef KM, Scattergood RO, Murty KL, Koch CC (2005) Appl Phys Lett 87:091904-1
12. Youngdahl CJ, Weertman JR, Hugo RC, Kung HH (2001) Scr Mater 44:1475
13. Lu L, Sui ML, Lu K (2000) Science 287:1463
14. Lu L, Wang LB, Ding BZ, Lu K (2000) J Mater Res 15:270
15. Koch CC (2003) J Meta Nano Mater 18:9
16. Weertman JR, Farkas D, Hemker KJ, Kung H, Mitra R, Swygenhoven H (1999) MRS Bull 24(2):44
17. Lu L, Li SX, Lu K (2001) Scr Mater 45:1163
18. Lu L, Sui ML, Lu K (2001) Acta Mater 49:4127
19. Lu L, Schwaiger R, Shan ZW, Dao M, Lu K, Suresh S (2005) Acta Mater 53:2169
20. Wang YM, Wang K, Pan D, Lu K, Hemker KJ, Ma E (2003) Scr Mater 48:1581
21. Huang Z, Gu LY, Weertman JR (1997) Scr Mater 37:1071
22. Dalla Torre F, Van Swygenhoven H, Victoria M (2002) Acta Mater 50:3957
23. Ebrahimi F, Bourne GR, Kelly MS, Matthews TE (1999) Nanostruct Mater 11:343
24. Ebrahimi F, Zhai Q, Kong D (1998) Scr Mater 39:315

25. Chen J, Wang W, Qian LH, Lu K (2003) Scr Mater 49:645
26. Malow TR, Koch CC, Margalia PQ, Murty KL (1998) Mater Sci Eng A252:36
27. Malow TR, Koch CC (1998) Acta Mater 46(18):6459
28. Jia D, Ramesh KT, Ma E, Lu L, Lu K (2001) Scr Mater 45:613
29. Guduru RK, Darling KA, Kishore R, Scattergood RO, Koch CC, Murty KL (2005) Mater Sci Eng A395:307
30. Guduru RK, Nagasekhar AV, Scattergood RO, Koch CC, Murty KL (2006) Met Mat Trans A 37A:1477
31. Toloczko MB, Kurtz RJ, Hasegawa A, Abe K (2002) J Nucl Mater 307–311:1619
32. Hamilton ML, Toloczko MB (2000) J Nucl Mater 283–287:488
33. Nomoto R, Carrick TE, John McCabe F (2001) Dent Mater 17:415
34. Kurtz SM, Jewett CW, Bergstrom JS, Foulds JR, Edidin AA (2002) Biomaterials 23:1907
35. Hankin GL, Toloczko MB, Hamilton ML, Faulkner RG (1998) J Nucl Mater 258–263:1651
36. Leo'n CA, Drew RAL (2002) Mater Lett 56:812
37. Hankin GL, Toloczko MB, Jhonson KI, Khaleel MA, Hamilton ML, Garner FA, Davies RW, Faulkner RJ (2000) ASTM STP 1366:1018
38. Wang Y, Chen M, Zhou F, Ma E (2002) Nature 419:912
39. Kocks UF, Argon AS, Ashby MF (1975) Thermodynamics and kinetics of slip, 1st edn. Pergamon Press, pp 255–260
40. Martin JL, Lo Piccolo B, Kruml T, Bonneville J (2002) Mater Sci Eng A 322:118
41. Wei QM, Jia D, Ramesh KT, Ma E (2002) Appl Phys Lett 81:1240